Rapid Imaging of Towed Streamer EM Data Using the Optimal Synthetic Aperture Method

Michael S. Zhdanov, Daeung Yoon, and Johan Mattsson

***Abstract*— The mainstream approach to the interpretation of towed streamer electromagnetic (EM) data is based on 2.5-D and/or 3-D inversions of the observed data into the resistivity models of the subsurface formations. However, the rigorous 3-D and even 2.5-D inversions require large amounts of computational power and time. The synthetic aperture (SA) method is one of the key techniques in remote sensing using radio frequency signals. During recent years, this method was also applied to low-frequency EM fields used for geophysical exploration. This letter demonstrates that the concept of the SA EM method can be extended for rapid imaging of the large volumes of towed streamer EM data. We introduce a notion of virtual receivers, which complement the actual receivers in the construction of the SA for the towed streamer data. A numerical study demonstrates that this method increases the EM response from potential subsurface targets and opens a possibility for on-board real-time imaging of EM data during a survey. The method is illustrated by the imaging of towed streamer EM data acquired over the Troll oil and gas fields in the North Sea. Remarkably, the imaging of the entire towed streamer EM survey requires just a few seconds of computation time on a desktop PC. This result is significant, because it opens a possibility for real-time imaging of the towed streamer EM survey data.**

***Index Terms*— Electromagnetic (EM), inversion, synthetic aperture (SA).**

I. Introduction

MARINE electromagnetic (EM) methods have found wide application in offshore hydrocarbon (HC) exploration because of their sensitivity to the resistive zones associated with the HC reservoirs, e.g., as shown in [1] and [2]. With the recent development of the towed streamer EM technology by PGS, marine EM surveys can be applied for rapid exploration of large areas in order to image the subsurface resistivity structure [3], [4]. However, interpretation of the multitransmitter and multireceiver EM data typical for towed streamer surveys is a very challenging problem, which usually requires a large-scale inversion of the observed data. In this situation, it is desirable to develop a rapid imaging technique for the towed streamer EM data for the reconnaissance surveying of the vast areas of the shelf. We propose for this purpose a concept of the synthetic aperture (SA), which has been widely used for processing and imaging of radio frequency EM and acoustic waves recorded by radars and sonars, respectively. The method is based on the idea that a virtual source constructed from different actual sources with specific radiation patterns can steer the interfered fields in the direction of an area of interest [5]–[8]. A similar approach has been introduced for diffusive EM fields [9]–[12], where the authors applied the SA method for the marine controlled-source EM (MCSEM) and towed streamer EM surveys by constructing an SA source to steer the generated fields in the direction of the resistive regions.

Another approach to achieving this goal has been introduced in [13] and [14], where the authors increased the sensitivity of the EM response to the resistive region using the concept of focusing controlled sensitivity by selecting the appropriate combination of the data weights.

In letters by Yoon and Zhdanov [15], [16], the authors introduced a concept of optimal SA by determining the optimal parameters of the SA for the node-based MCSEM data, which enhances the EM anomaly from a resistive region located in either deep or shallow marine environments. Note that the conventional MCSEM survey configuration uses fixed-node sea-bottom receivers and moving transmitters. In this latter study, we develop an optimal SA method for towed streamer EM survey data with transmitter and receivers towed behind a vessel. This demonstrates that the developed method increases the EM response from the potential subbottom targets significantly, which can be effectively used in reconnaissance surveys for finding the locations of HC reservoirs.

II. Virtual Receivers

A towed streamer EM survey consists of a set of transmitter and receivers towed by a vessel, while the MCSEM survey deploys fixed receivers at the sea floor. This means that in the latter system, the receiver positions are the same for all the different transmitter shots, but in the former system, the receiver positions for one transmitter shot are different from those for another shot. The fundamental concept of the SA method is that the signals generated at different source positions are measured at the same receiver positions, so that they can be integrated to increase the potential anomaly. Unlike the conventional MCSEM system, the towed streamer system consists of a set of towed receivers, which can measure a signal generated at a certain transmitter position only. In order to integrate the signals generated by different sources at the

Manuscript received June 22, 2016; revised November 8, 2016; accepted December 1, 2016. Date of publication December 29, 2016; date of current version January 19, 2017.This work was supported in part by the University of Utah Consortium for Electromagnetic Modeling and Inversion, in part by Techno Imaging, in part by MFTI, and in part by Petroleum Geo-Services.

M. S. Zhdanov is with The University of Utah, Salt Lake City, UT 84112 USA, also with Techno Imaging, Salt Lake City, UT 84107 USA, and also with the Moscow Institute of Physics and Technology, 141701 Dolgoprudny, Russia (e-mail: michael.s.zhdanov@gmail.com).

D. Yoon is with The University of Utah, Salt Lake City, UT 84112 USA, and Techno Imaging, Salt Lake City, UT 84107 USA (e-mail: duyoon@gmail.com).

J. Mattsson is with PGS, 0283 Oslo, Norway (e-mail: johan.mattsson@pgs.com).

Color versions of one or more of the figures in this letter are available online at http://ieeexplore.ieee.org.

Digital Object Identifier 10.1109/LGRS.2016.2637919

same receiver positions in the towed streamer EM system, we have to interpolate and/or extrapolate the fields from each source to the virtual receiver positions, which can be shared by all the transmitter shots. Note that the concept of virtual receiver is also quite common in radar applications.

Consider a typical towed streamer EM survey consisting of a set of towed receivers with the transmitter–receiver offset index, $s = 1, 2, \ldots, S$. A long bipole transmitter generates a low-frequency EM field from points with coordinates $\tilde{r}_j$, $j = 1, 2, \ldots, J$. The data recorded at the receivers by a transmitter located at point $\tilde{r}_j$ can be presented as a vector-column, $\mathbf{d}_j = [d_j^{(1)}, d_j^{(2)}, \ldots, d_j^{(S)}]^T$, where $d_j^{(s)}$ is the data observed at offset s from the transmitter located at the point $\tilde{r}_j$.

In the marine environment, the measured electric field decays quickly with an increase in the distance (offset) between the transmitter and the receiver, which makes it difficult to detect an anomaly related to an HC reservoir. In order to overcome this problem, the observed data are usually normalized by the amplitude of the background field data as follows:

$$d_j^{N(s)} = d_j^{(s)} / \left| d_j^{b(s)} \right| \tag{1}$$

where $d_j^{(s)}$ and $d_j^{b(s)}$ describe the total and background field data, respectively, recorded at offset s from the transmitter located at the point $\tilde{\mathbf{r}}_j$.

There are different ways to determine the background field. One way is based on the 1-D inversion of the observed data. In this case, the background field is determined as a field generated by a given transmitter in some background geoelectrical models, which is usually selected as a horizontally layered model [17]. Another way uses the reference field in the observation point far enough from the region of interest, which does not require any model to calculate the background field. Indeed, if we know that some measurements are made outside the location of the interesting area, we can consider these data as a background (reference) field, $\mathbf{d}^b = \mathbf{d}_j^{\text{ref}} = [d_j^{\text{ref}(1)}, d_j^{\text{ref}(2)}, \ldots, d_j^{\text{ref(S)}}]^T$, $j = 1, 2, \ldots, J$.

In order to apply the optimal SA method, we first determine the positions of the virtual receivers to be shared by all the transmitters. For simplicity, we select the corresponding virtual receiver positions to be the same as all actual receiver positions for all transmitters. If we assume that there are no exactly overlapped receiver positions for different sources in the original data, there will be $L = JS$ actual and virtual receiver positions with coordinates, denoted as follows: $\mathbf{r}_l, l = 1, 2, \ldots, L$. We use a linear interpolation of the data from the actual to the virtual receivers, if the virtual receivers are located within the maximum offset from the corresponding transmitter, and we use an extrapolation, if the virtual receivers are located outside this range. More specifically, the normalized observed data are linearly interpolated from the closest actual receivers into the virtual receiver positions for each source position j, forming an $[L \times 1]$ vector-column, $\mathbf{d}_j^N = [d_j^{N(1)}, d_j^{N(2)}, \ldots, d_j^{N(L)}]^{\mathbf{T}}$ (where $j = 1, 2, \ldots, J$), if the values $d_j^{N(l)}$ corresponds to the range within the maximum offset from the corresponding transmitter, $\tilde{\mathbf{r}}_j$. The values $d_j^{N(l)}$ corresponding to the range exceeding the maximum offset from the corresponding transmitter, $\tilde{\mathbf{r}}_j$, are obtained by extrapolating from the actual receivers. However, for simplicity, we set the extrapolated values to be 1 (a unit), because the normalized data are equal to 1 everywhere outside the anomaly (assuming that the observed data are equal to the reference background field outside the anomaly).

Combining all the normalized data for all transmitters, we obtain a $[JL \times 1]$ vector-column of the data recorded in both the actual and virtual receivers

$$\mathbf{d}^N = \left[\mathbf{d}_1^N, \mathbf{d}_2^N, \mathbf{d}_3^N, \ldots, \mathbf{d}_J^N\right]^T. \tag{2}$$

III. Optimal Synthetic Aperture for Towed Streamer EM Survey

It was demonstrated in [16] that the SA data can be calculated as a linear combination of the responses for all the transmitters

$$\mathbf{d}_A = \mathbf{W}_A \mathbf{d}^N \tag{3}$$

where $\mathbf{d}_A = [d_A^{(1)}, d_A^{(2)}, d_A^{(3)}, \ldots, d_A^{(L)}]^T$ is an $[L \times 1]$ vector-column of the SA data based on the normalized observed data. $\mathbf{W}_A$ is an $[L \times JL]$ block-diagonal rectangular matrix of the weights

$$\mathbf{W}_A = \begin{bmatrix} \mathbf{w}^T & 0\cdots & 0\cdots & 0\cdots \\ 0\cdots & \mathbf{w}^T & 0\cdots & 0\cdots \\ 0\cdots & 0\cdots & \ddots & 0\cdots \\ 0\cdots & 0\cdots & 0\cdots & \mathbf{w}^T \end{bmatrix}. \tag{4}$$

In the last formula, $\mathbf{w}$ is a $[J \times 1]$ vector-column of the corresponding SA weights, w_j, $\mathbf{w} = [w_1, w_2, \ldots, w_J]^T$. The goal is to find the optimal values of the weights, w_j, which would enhance the EM anomalies from the resistive regions. Note that, the towed streamer EM system measures the inline component of the electric field, E [3], [4]. In this case, following [16], we can write (3) as follows:

$$\mathbf{d}_A = \mathbf{E}^N \mathbf{w} \tag{5}$$

where $\mathbf{E}^N$ is an $[L \times J]$ matrix of the normalized inline components of the electric fields, $E_j^{N(l)}$, recorded by a virtual receiver at point $\mathbf{r}_l$ for a transmitter, $\tilde{\mathbf{r}}_j$

$$\mathbf{E}^N = \begin{bmatrix} E_1^{N(1)} & E_2^{N(1)} & \cdots & E_J^{N(1)} \\ E_1^{N(2)} & E_2^{N(2)} & \cdots & E_J^{N(2)} \\ \vdots & \vdots & \ddots & \vdots \\ E_1^{N(L)} & E_2^{N(L)} & \cdots & E_J^{N(L)} \end{bmatrix}. \tag{6}$$

By analogy with (5), the SA response for the normalized background electric field can be expressed as $\mathbf{d}_B = \mathbf{E}^{Nb}\mathbf{w}$, where $\mathbf{d}_B$ is an $[L \times 1]$ vector-column and $\mathbf{E}^{Nb}$ is an $[L \times J]$ matrix of the normalized background electric fields at the virtual receivers, with the scalar components, determined as follows:

$$E_j^{Nb(l)} = E_j^{b(l)} / \left| E_j^{b(l)} \right|, \quad l = 1, 2, \ldots, L; \;\; j = 1, 2, \ldots, J. \tag{7}$$

We also introduce vector-column, $\mathbf{d}_R$ of the ratio between the SA data and the SA response for the normalized background electric field

$$\mathbf{d}_R = \left[\frac{d_A^{(1)}}{d_B^{(1)}}, \frac{d_A^{(2)}}{d_B^{(2)}}, \ldots, \frac{d_A^{(L)}}{d_B^{(L)}}\right]^T = \mathbf{A}(\mathbf{w})$$
$$d_A^{(l)} d_B^{(l)} = \left[\sum_{j=1}^{J} E_j^{N(l)} w_j\right] \Big/ \left[\sum_{j=1}^{J} E_j^{Nb(l)} w_j\right] \quad (8)$$

where $\mathbf{A}$ is a forward operator for the normalized SA data $\mathbf{d}_R$, which is a function of the SA weights $\mathbf{w}$. Note that, if all the SA weights $\mathbf{w}$ are equal to 1, then according to [16], the corresponding data $\mathbf{d}_R$ are called the *SA data without steering*. $\mathbf{d}_R$ values computed based on the optimal SA weights are called *optimal SA data*.

It was shown in [16] that one can find the optimal SA weights by solving a minimization problem for the corresponding parametric functional

$$P(\mathbf{w}) = \|\mathbf{D} - \mathbf{A}(\mathbf{w})\|^2 + \alpha \|\mathbf{w} - \mathbf{w}_{\text{apr}}\|^2 = \min \quad (9)$$

where $\mathbf{D}$ is a so-called *designed SA (DSA)*, α is a regularization parameter, and $\mathbf{w}_{\text{apr}}$ is an *a priori* vector-column of the data weights, which, for simplicity, can be selected as follows: $\mathbf{w}_{\text{apr}} = [1,1,\ldots,1]^T$. The DSA, according to its name, is selected (designed) with the purpose of enhancing the EM anomalies from the potential targets. In the case of a reconnaissance survey, it is reasonable to select a uniform DSA with the constant value greater than one to enhance the anomalies, present in the survey area. Note that, in the case of a uniform DSA, all anomalies different from the background increase in the optimal SA data after minimization of the functional. The minimization problem in (9) is solved using the regularized conjugate gradient method [16], [18].

IV. Selection of a Designed Normalized Synthetic Aperture Data

A. Selection of a Designed Normalized Synthetic Aperture Data

We should note that different selections of the DSA, for the optimal SA method, can result in different optimal SA weights. In this section, we discuss how the different DSAs affect the results and make the recommendations on their selections.

Consider a geoelectrical model consisting of 300-m seawater layer with a resistivity of 0.33 and 1-Ω-m half space of sediment. A reservoir with sizes of 4 km × 4 km × 200 m is located at a depth of 800 m below the sea floor, and the resistivity of the reservoir is 100 Ωm [Fig. 1(a)]. Note that the ratio of the resistivity of the reservoir to the resistivity of the sediment is equal to 100. The towed streamer EM survey consists of one survey line, running in the x-direction at $y = 0$. The horizontal electric dipole transmitter oriented in the x-direction with a moment of 1 Am is towed from 20 to −20 km in the x-direction at a depth of 10 m below the sea surface. Sixty receivers with offsets between 900 and 7720 m are towed at a depth of 100 m and

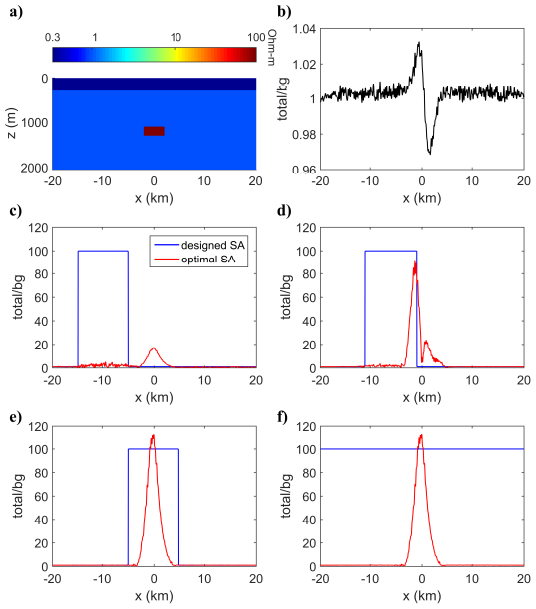

Fig. 1. (a) Sketch of Model 1. (b) SA data without steering. The observed data were contaminated with the random 10% Gaussian noise. (c)–(e) Plots of the optimal SA data (red lines) obtained using a boxcar function with different locations (blue lines) as a DSA. (f) Plot of the optimal SA data (red line) obtained using a uniform DSA (blue line).

measure inline electric fields at a frequency of 0.4 Hz. The data were contaminated with the random 10% Gaussian noise.

In order to apply the optimal SA method, we construct an SA source using all the transmitter points on the survey line, and select the background (reference) field as the observed data generated by the very first transmitter located at $x = 20$ km. Fig. 1(b) shows the plot of the normalized SA data without steering. We have considered four different DSAs in order to demonstrate how they affect the optimal SA data. We first select a boxcar function as the DSA, setting the maximum value equal to 100 (we call this value *an amplification factor*) within the area of the expected reservoir anomaly and to 1 outside of the targeted zone. Thus, the amplification factor of the DSA is equal to the ratio of the resistivity of the reservoir to the resistivity of the sediment in Model 1. Then, we move the boxcar function along the axis x, as shown in Fig. 1(c)–(e). Fig. 1(c) demonstrates that if there is no anomalous field within the area of the maximum of the boxcar function, the optimal SA method does not generate any false anomaly. Fig. 1(d) and (e) indicates that the boxcar function has to fully cover the area of the anomalous field, otherwise only the anomalous fields inside the boxcar area increase. Finally, we use a constant value for the DSA. As demonstrated in [16], the optimal SA method increases or decreases the SA data only within the area, where the true anomaly exists. Therefore, one can simply use a constant value for the DSA in order to enhance the responses from all potential targets. Fig. 1(f) presents a plot of the optimal SA data (red line) obtained using a uniform DSA (blue line). One can see that the optimal SA data shown in Fig. 1(e) and (f) are practically identical. This result illustrates the fact that the uniform SA can be successfully used in the reconnaissance towed streamer

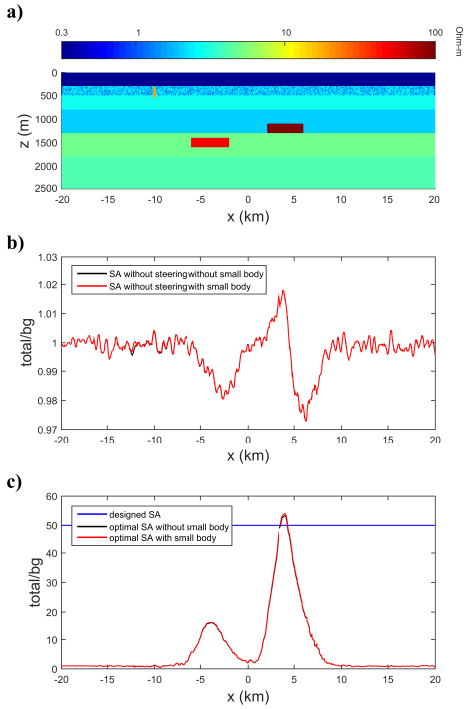

Fig. 2. (a) Sketch of Model 2. (b) SA data without steering with (red line) and without (black line) the small resistive body. (c) Plot of the optimal SA data with (red line) and without (black line) the small resistive body obtained using a uniform DSA (blue line).

EM survey, where the location of the potential target is not *a priori* known.

B. Model With Near-Seafloor Inhomogeneities

We consider a complex model, which consists of two thin reservoirs and near-seafloor inhomogeneities. Model 2 consists of 300-m seawater with a resistivity of 0.33 Ωm and five conductive sediment layers, as shown in Fig. 2(a). The first top sediment layer with a thickness of 200 m represents the near-seafloor inhomogeneities, with resistivities varying randomly from 1 to 4 Ωm. The first layer also contains a small resistive body with a size of 200 m × 200 m × 200 m and a resistivity of 20 Ωm, as shown in Fig. 2(a). The resistivities of the second sediment layer and below including the bottom half space are 3, 2, 5, and 4 Ωm, respectively. The reservoirs have the same size of 4 km × 4 km × 200 m but they are located at different depths of 1100 m (the left reservoir) and 800 m (the right reservoir) below the sea surface, with resistivities of 50 and 100 Ωm, respectively, as shown in Fig. 2(a). The separation between the reservoirs is 4 km in the x-direction. The EM survey configuration is the same as that considered in Model 2. The data were contaminated with the random 10% Gaussian noise.

As was done above for Model 1, we first construct an SA source using all the transmitters in the survey line, and select the background (reference) field as the observed data generated by the very first transmitter located at $x = 20$ km. Then, we plot the normalized SA data without steering, as shown in Fig. 2(b). In this complex model, the SA data without steering are distorted due to the near-surface inhomogeneities

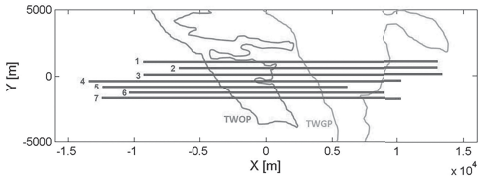

Fig. 3. Configuration of the towed streamer EM survey conducted in the TWOP and TWGP. Black solid lines: locations of the seven survey lines.

and the noise in the observed data, which makes it difficult to determine the locations of the targets from the anomalous responses in the plot of the SA data without steering.

As discussed in Section IV-A, we select a uniform DSA [shown by a blue line in Fig. 2(c)] with the amplification factor of 50, equal to the ratio of the resistivity of the shallow reservoir to the resistivity of the corresponding sediment layer in Model 2. After applying the optimal SA method to the observed data, we have generated optimal SA data shown by the red line. One can see that the anomalies of the SA data increased over the reservoirs, while the magnitude of the data elsewhere remains practically the same as for the SA data without steering. As one can see, the areas of the increased anomalies agree well with the true horizontal locations of the targets. We have also compared the results of the application of the SA without steering and optimal SA to the data with and without the small resistive body, as shown in Fig. 2(b) and (c), respectively. As one can see, the effect of the small body in the near-surface layer is negligible.

V. Application of the Optimal Synthetic Aperture Method to the Towed Streamer EM Data Collected in the Troll West Oil and Gas Provinces

We applied the optimal SA method to the towed streamer EM data collected in the Troll West Oil Province (TWOP) and Troll West Gas Province (TWGP). These data were studied in [19]–[21], where a rigorous 3-D inversion was conducted for these data, making them a suitable data set for testing the optimal SA method.

The towed streamer EM data used in our numerical study were collected at seven survey lines at a frequency of 0.496 Hz. Fig. 3 shows the seven survey lines over the true locations of TWOP and TWGP. The 8700-m-long EM streamer was towed at a depth of 100 m below the sea surface. Eleven receivers with offsets between 1860 and 7554 m were selected. The electric current source was towed at a depth of 10 m below the sea surface.

We applied the optimal SA method to the data collected at all the lines 1–7. The reference field was selected using a set of the observed data generated by the first transmitter located at the left end of line #1, assuming that this field was least affected by the anomalous resistivity of the Troll oil and gas fields. In our choice of the least affected location, we considered the towing direction of the streamer, which was from the left to the right for lines # 1–3, and from the right to the left for lines # 4–7. This reference field was used as the background field for all the towed streamer EM data collected in all seven lines. We should also note that, in practice, we recommend selecting several different locations

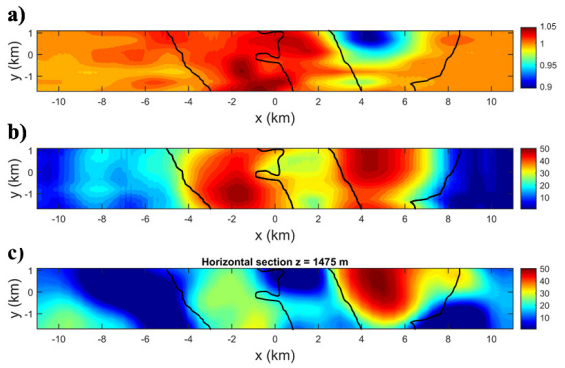

Fig. 4. (a) and (b) Maps of the SA data without steering and the optimal SA data, respectively, with the known reservoir extents (black solid line). (c) Horizontal section of the inversion results for the same data at a depth of 1475 m, produced by conventional 3-D regularized inversion [21].

of the reference receiver to determine the one least affected by the anomalous resistivity.

To apply the optimal SA method to the Troll data, we first selected a uniform DSA with the amplification factor of 50, which was selected based on an estimated ratio of the resistivity of the HC reservoir to the resistivity of surrounding sediments in the survey area. Fig. 4(a) and (b) shows the maps of the normalized SA data without steering and the optimal SA data, respectively. As one can see, the optimal SA method increases the observed SA data significantly and provides the anomalies, which correlate well with the boundaries of the known HC reservoirs. Fig. 4(c) shows a horizontal section of the inversion results for the same data at a depth of 1475 m, produced by conventional 3-D regularized inversion [21]. The depth of 1475 m was selected, because 3-D inversion result showed the highest values of resistivity of the two reservoirs at this depth, which agreed well with the depth of the targets estimated based on seismic data. As one can see, the map of optimal SA data agrees very well with the true horizontal locations of HC reservoirs of the TWOP and TWGP (black outlines) as well as the inversion result. This case study demonstrates the remarkable effectiveness of the optimal SA method to find the horizontal locations of the targets without any inversion. Another advantage of this method is its very short computational time. We computed the optimal SA data using a personal computer (PC) with Intel Core i7, 32 GB, and 2.5 GHz, in less than a few seconds, while a rigorous 3-D inversion required several hours or even days of computation on a PC cluster. Note that the computational time mostly depends on the number of data points, which were about 40 000 in this case. Thus, the optimal SA method can be considered as an effective technique for real-time scanning of the survey area for potential HC reservoirs using the EM data.

VI. Conclusion

We have introduced a novel method for fast imaging of the towed streamer EM data based on the concept of the optimal SA. It has been shown that this method increases the EM response from potential sea-bottom HC reservoirs significantly. A case study with towed streamer EM data acquired over the Troll oil and gas fields in the North Sea has demonstrated the effectiveness of the optimal SA method in mapping the sea-bottom resistive targets (e.g., HC reservoirs). The method is extremely fast, and the computational time on a standard PC is less than a few seconds for large survey data (up to 40 000 observation points). The optimal SA method, however, cannot substitute the conventional 3-D inversion, which should be applied to all anomalies, discovered by this technique, to resolve the true nature of the targets. At the same time, the developed innovative technique can be used as a fast data processing technique for on-board real-time evaluation of the data collected in a reconnaissance towed streamer EM survey with the goal of scanning a vast area of the marine shelf.

References

[1] J. Hesthammer, A. Stefatos, M. Boulaenko, S. Fanavoll, and J. Danielsen, "CSEM performance in light of well results," *Leading Edge*, vol. 29, no. 1, pp. 34–41, 2010.
[2] S. Constable, "Ten years of marine CSEM for hydrocarbon exploration," *Geophysics*, vol. 75, no. 5, pp. 75A67–75A81, 2010.
[3] F. Engelmark, J. Mattsson, and J. Linfoot, "Marine CSEM with a novel towed acqusition system," in *Proc. PGCE*, 2012, pp. 345–350.
[4] A. Mckay, J. Mattson, and Z. Du, "Towed streamer EM—Reliable recovery of sub-surface resistivity," *First Break*, vol. 33, no. 4, pp. 75–85, 2015.
[5] S. R. DeGraaf, "SAR imaging via modern 2-D spectral estimation methods," *IEEE Trans. Image Process.*, vol. 7, no. 5, pp. 729–761, May 1998.
[6] M. Cheney, "A mathematical tutorial on synthetic aperture radar," *SIAM Rev.*, vol. 43, no. 2, pp. 301–312, 2001.
[7] M. Çetin and W. C. Karl, "Feature-enhanced synthetic aperture radar image formation based on nonquadratic regularization," *IEEE Trans. Image Process.*, vol. 10, no. 4, pp. 623–631, Apr. 2001.
[8] A. I. Korobov, M. Y. Izosimova, and S. A. Toschov, "Development of ultrasound focusing discrete array for air-coupled ultrasound generation," *Phys. Procedia*, vol. 3, no. 1, pp. 201–207, 2010.
[9] Y. Fan *et al.*, "Synthetic aperture controlled source electromagnetics," *Geophys. Res. Lett.*, vol. 37, no. 13, p. L13305, 2010.
[10] Y. Fan *et al.*, "Increasing the sensitivity of controlled-source electromagnetics with synthetic aperture," *Geophysics*, vol. 77, no. 2, pp. E135–E145, 2012.
[11] A. Knaak, R. Snieder, Y. Fan, and D. Ramirez-Mejia, "3D synthetic aperture and steering for controlled-source electromagnetics," *Leading Edge*, vol. 32, no. 8, pp. 972–978, 2013.
[12] J. Mattsson and F. Engelmark, "Optimized synthetic aperture sensitivity enhancement of a deep EM marine target," in *Proc. 75th Conf. Exhibit., EAGE, Extended Abstracts*, 2013, pp. 3446–3450.
[13] D. Yoon and M. S. Zhdanov, "Controlled sensitivities for marine CSEM surveys," in *Proc. 81st Annu. Int. Meeting, SEG, Expanded Abstracts*, 2011, pp. 599–603.
[14] M. S. Zhdanov, "Focusing controlled sensitivity of geophysical data," *J. Geol. Geosci.*, vol. 10, pp. 1–5, Mar. 2013.
[15] D. Yoon and M. S. Zhdanov, "An optimal synthetic aperture method for the creation of directional sensitivity and removal of the airwave effect in MCSEM data," in *Proc. 84th Annu. Int. Meeting, SEG, Expanded Abstracts*, 2014, pp. 685–690.
[16] D. Yoon and M. S. Zhdanov, "Optimal synthetic aperture method for marine controlled-source EM surveys," *IEEE Geosci. Remote Sens. Lett.*, vol. 12, no. 2, pp. 414–418, Feb. 2015.
[17] M. S. Zhdanov, *Geophysical Electromagnetic Theory and Methods*, vol. 43. New York, NY, USA: Elsevier, 2009.
[18] M. S. Zhdanov, *Inverse Theory and Applications in Geophysics*. New York, NY, USA: Elsevier, 2015.
[19] M. S. Zhdanov *et al.*, "Three-dimensional inversion of towed streamer electromagnetic data," *Geophys. Prospecting*, vol. 62, no. 3, pp. 552–572, 2014.
[20] M. S. Zhdanov, M. Endo, D. Yoon, M. Čuma, J. Mattsson, and J. Midgley, "Anisotropic 3D inversion of towed-streamer electromagnetic data: Case study from the Troll West Oil Province," *Interpretation*, vol. 2, no. 3, pp. SH97–SH113, 2014.
[21] D. Yoon, M. S. Zhdanov, J. Mattsson, H. Cai, and A. Gribenko, "A hybrid finite-difference and integral-equation method for modeling and inversion of marine controlled-source electromagnetic data," *Geophysics*, vol. 81, no. 5, pp. E323–E336, 2016.